

Water Resources Research

RESEARCH ARTICLE

10.1029/2022WR032338

Key Points:

- Hungry-water-driven channel erosion causes the sharp reduction in low-flow water-levels
- Floodplain resistance increase dominates the minor change in high-flow water-levels, followed by riverbed coarsening and greater fluctuations in the river longitudinal profile
- Floodplain resistance increase mainly caused by vegetation expansion in floodplain and channel bars due to the reduced floodplain submerged frequency

Supporting Information:

Supporting Information may be found in the online version of this article.

Correspondence to:

J. Deng,
dengjinyun@whu.edu.cn



Citation:

Hu, Y., Li, D., Deng, J., Yue, Y., Zhou, J., Chai, Y., & Li, Y. (2022). Mechanisms controlling water-level variations in the Middle Yangtze River following the operation of the Three Gorges Dam. *Water Resources Research*, 58, e2022WR032338. <https://doi.org/10.1029/2022WR032338>

Received 9 MAR 2022

Accepted 11 SEP 2022

Mechanisms Controlling Water-Level Variations in the Middle Yangtze River Following the Operation of the Three Gorges Dam

Yong Hu¹ , Dongfeng Li² , Jinyun Deng¹ , Yao Yue¹ , Junxiong Zhou³, Yuanfang Chai⁴ , and Yitian Li¹

¹State Key Laboratory of Water Resources and Hydropower Engineering Science, Wuhan University, Wuhan, China,

²Department of Geography, National University of Singapore, Kent Ridge, Singapore, ³Department of Bioproducts and Biosystems Engineering, University of Minnesota Twin Cities, St Paul, MN, USA, ⁴Department of Earth Sciences, Vrije Universiteit Amsterdam, Amsterdam, The Netherlands

Abstract Understanding the mechanisms controlling downstream water-level variations after the operation of the Three Gorges Dam is important for riverine flood and drought management. However, our quantitative understanding of the multiple controls of river morphology, vegetation, and floodplain resistance on water levels in the Middle Yangtze River (MYR) remains limited. Here, we analyze changes in river channels and floodplain resistance in the MYR using 450 cross-sectional profiles as well as data on discharge, water levels, sediment, and satellite images from 2003 to 2015. Results show an overall decline in low-flow water-levels (at a given small discharge) due to severe incisions of low-flow channels caused by a sharp reduction of ~90% in sediment loads from 1950–2002 to 2003–2020. In contrast, high-flow water-levels (at a given large discharge) display minor changes. Our analysis shows that the notably increased floodplain resistance due to vegetation growth is likely the dominant factor elevating flood water-levels, followed by riverbed coarsening and greater fluctuations in the river longitudinal profiles. Our findings further the understanding of downstream geomorphic response to dam operation and their impacts on water levels and have important implications for riverine flood management in dammed river systems.

1. Introduction

Half a century ago, Leopold (1956) predicted that dams would someday become so numerous on American rivers that they would be the primary factor controlling the characteristics of river channels. His prediction is becoming true for river systems worldwide, with > 45,000 large dams (height > 15 m) distributed over 140 countries (Ma et al., 2022; Syvitski et al., 2022). Dams are often designed to generate hydropower and mitigate floods (Li et al., 2022; Ma et al., 2022), but they also disrupt river continuity and induce drastic temporal and spatial alterations in river flow and sediment regimes (Li et al., 2018, 2021; Zhou et al., 2020). Such flow-sediment regime adjustments following dam construction have caused substantial downstream geomorphological, ecological, and societal changes (Best, 2019; Darby et al., 2016; Latrubesse et al., 2017; Schmitt et al., 2018; Syvitski et al., 2022). Recent studies suggest that dams could amplify floods in some rivers such as the Yellow River (Ma et al., 2022).

Drought and flood risks are typically evaluated by the water levels in the low- and high-flow inundation extents (stages at a given small or large discharge). Changes in river water levels reflect the dynamics and geometry of rivers, and have consequently been studied for the purposes of flood control, water supply, waterway navigation, and aquatic ecosystems (Chai et al., 2020; Doyle & Harbor, 2003; Gierszewski et al., 2020). Variations in high- and low-flow water levels (stages at a given large or small discharge) downstream of dams have been documented in many rivers worldwide, and variation trends in high- and low-flow water levels are different mainly due to channel erosion, riverbed coarsening, floodplain adjustments, and river regulation works (Bormann et al., 2011; Ma et al., 2022; Park, 2020). For instance, both low- and high-flow water levels decreased on the Lower Mississippi River, mainly the result of artificial cutoffs in the late 1920s and 1930s (Jemberie et al., 2008). In addition, increased high-flow water levels in Lower Missouri River were correlated strongly with river modifications such as navigation dikes and levees (Pinter et al., 2008). The decrease in low-flow water levels and the increase in high-flow water levels in the Fulda River were interpreted by the channel-bed incision due to construction of groynes, combined with decreased capacity to convey large flows due to decreased flow velocity and reduced cross-sectional area in response to construction of dikes, bridges, and other channel and floodplain structures

(Bormann et al., 2011). Furthermore, the Mississippi River flooded with a discharge in 2011 lower than that measured in previous floods, but due to the backwater caused by dense vegetation in the floodplain, the high-flow water level increased (Carle et al., 2015; Day et al., 2016). Recently, amplified high-flow water levels in the lower Yellow River mainly related to bed incision is accompanied by sediment coarsening, which facilitates development of large dunes that increase flow resistance and reduce velocity relative to pre-dam conditions (Ma et al., 2022).

Here, we aim to investigate the mechanisms controlling downstream water-level variations following the operation of the Three Gorges Dam (TGD). Specifically, we employ cross-sectional profiles, hydrological datasets, and remote-sensing images for the Middle Yangtze River (MYR) covering both the pre- and post-TGD periods. The specific objectives of the study are to (a) analyze the spatial and temporal trends in water levels in high- and low-flow inundation extents (stages at a given large or small discharge; Figure 1c), and (b) investigate the mechanisms controlling water-level changes with a focus on morphology dynamics and changes in flow resistance.

2. Study Area

The Yangtze River is the third-longest river in the world with a total length of ~6,300 km and is generally divided into the upper, middle, and lower reaches based on different hydrological characteristics and geographical conditions (Cao & Wang, 2015). The MYR extends between the Yichang and Hukou reaches ~955 km immediately downstream of the TGD and includes the floodplain-type lakes of Dongting and Poyang (Xia et al., 2017) (Figure 1). These lakes indeed now function as tributaries to the Yangtze River and create some backwater effect in the river channel. The jacking force is an interactive force in that the lakes create a backwater effect on the Yangtze River and in turn, the Yangtze River has a block effect on the outlet of lakes. The MYR is a predominantly meandering channel with many floodplains, and a riverbed composition that tends toward finer grain sizes downstream (He et al., 2021; Lyu et al., 2020).

Here, we discuss the three periods summarized in Table 1, which reflect the different sediment and flow regimes in the MYR caused by the operation of the TGD (Zheng, 2016). Nine sub-reaches (Yichang-Zhicheng, Zhicheng-Majiadian, Majiadian-Shashi, Shashi-Shishou, Shishou-Jianli, Jianli-Chenglingji, Chenglingji-Hankou, Hankou-Jiujiang, and Jiujiang-Hukou; Figure 1 and Table 1) were divided based on the local geographical settings and channel patterns. Sediment and flow fluxes in every sub-reach were measured at 18 hydrometric stations (Figure 1 and Table 1).

3. Materials and Methods

3.1. Data Sources

All the original raw data used in this study (except Landsat images) were obtained from the Changjiang Water Resources Commission (CWRC), namely hydrological and sediment data (i.e., daily mean discharge, water levels, and sediment concentrations at multiple hydrometric stations; Figure 1), topographical data that is, annual one-dimensional cross-sectional profiles at 450 specific locations (Table S1 in Supporting Information S1 measured using a multi-beam echo-sounder), and riverbed sediment grain-size data, as summarized in Table 2. Before these datasets are released to the public, they undergo rigorous verification and uncertainty analysis following government protocols, such as protocol for liquid flow measurement in open channels; protocol for measurements of suspended sediment in open channels; and protocol for port and waterway engineering survey, published by the Ministry of Water Resources, China. Detailed descriptions of the sampling methods and uncertainties in these hydrology and cross-sectional topography data can be found in Li et al. (2019) and thus not repeated here.

Landsat-8 Operational Land Imager and Landsat-5 Thematic Mapper data were obtained from the United States Geological Survey with a spatial resolution of 30 m. Six specific scenes were acquired to cover the entire study reach, and 16 relatively stable and large floodplains were chosen for analysis (Figure 1 and Table 1). Such satellite data are used to calculate the Normalized Difference Vegetation Index (NDVI) to reflect the vegetation change from 2003 to 2015 (Figure 11).

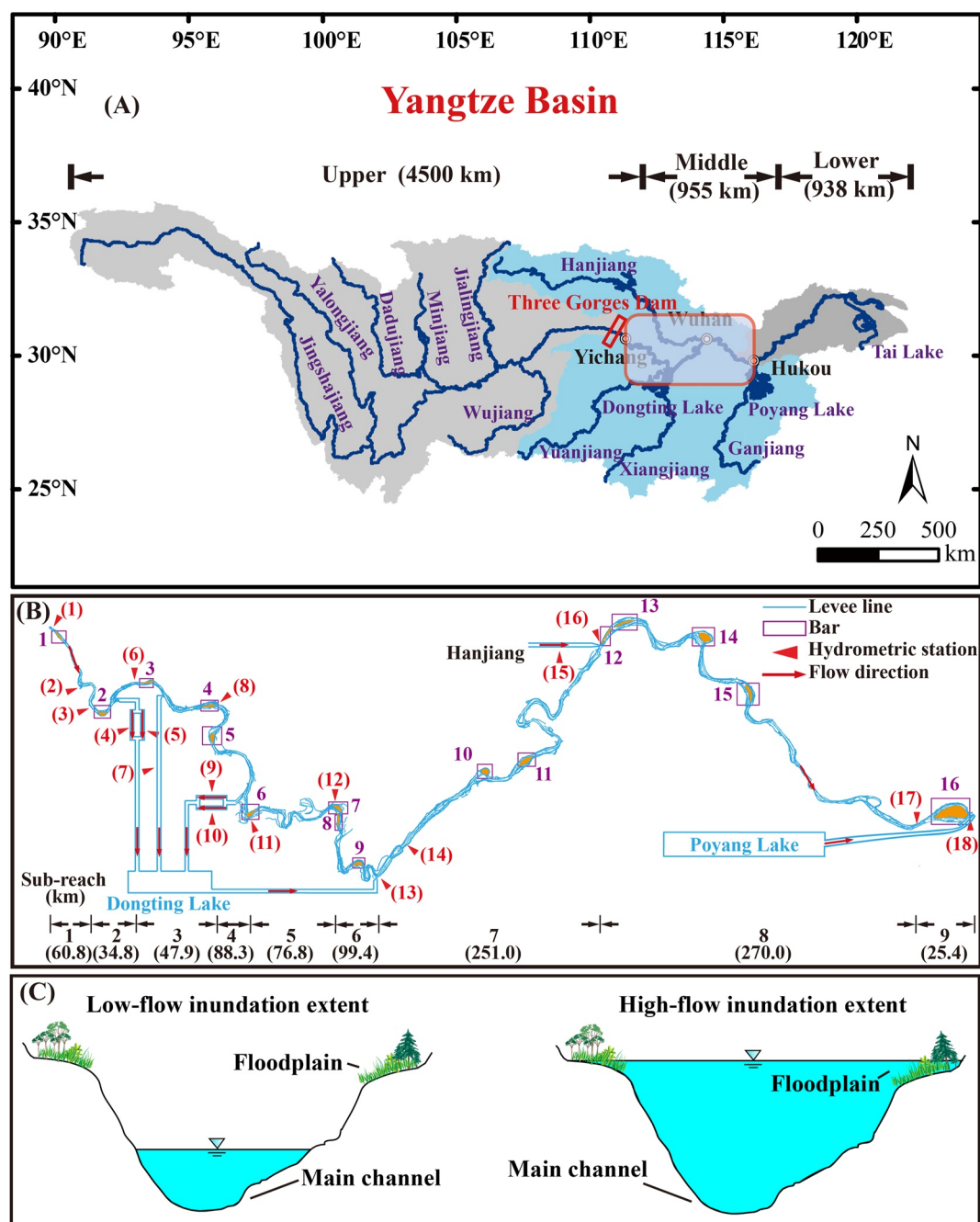


Figure 1. Sketch map of the study area: (a) the Yangtze River Basin, (b) the Middle Yangtze River with locations of hydrometric stations, floodplains, and diversion inlets, and (c) sketch map of the low- and high-flow inundation extents.

3.2. Sediment Balance Method

The cross-sectional topography method is widely used to investigate geomorphic changes in channels and can, therefore, be applied to calculate the amount of erosion and deposition (Xia et al., 2016). The calculation equation (Equation 1) is expressed as follows:

$$V = \sum_{i=1}^{n-1} \frac{1}{3} \left(\Delta A_i + \Delta A_{i+1} + \sqrt{\Delta A_i + \Delta A_{i+1}} \right) \times \Delta L_i \quad (1)$$

where V is the erosion (+) or deposition (−) volume, A_i is the i th cross-sectional area, ΔA_i is the area change at the i th cross-section, and ΔL_i is the distance between the i th and $(i + 1)$ th cross-sections.

Table 1
Essential Information on Eighteen Hydrometric Stations, Sixteen Floodplains, and Nine Sub-Reach in the Middle Yangtze River (MYR) and Three Operation Periods of the Three Gorges Dam (TGD)

Station number	Station name	Floodplain number	Floodplain name	Channel number	Included reaches	Length
1	Yichang	1	Yanzhi	Sub-reach 1	Yichang-Zhicheng	60.8 km
2	Yidu	2	Guan	Sub-reach 2	Zhicheng-Majiadian	34.8 km
3	Zhicheng	3	Liutiao	Sub-reach 3	Majiadian-Shashi	47.9 km
4	Xinjiangkou	4	Lalin	Sub-reach 4	Shashi-Shishou	88.3 km
5	Shadaoguan	5	Tuqi	Sub-reach 5	Shishou-Jianli	76.8 km
6	Majiadian	6	Ouchikou	Sub-reach 6	Jianli-Chenglingji	99.4 km
7	Mituosi	7	Wugui	Sub-reach 7	Chenglingji-Hankou	251 km
8	Shashi	8	Dama	Sub-reach 8	Hankou-Jiujiang	270 km
9	Kangjiagang	9	Xiongjia	Sub-reach 9	Jiujiang-Hukou	25.4 km
10	Guanjiapu	10	Zhong			
11	Shishou	11	Fuxing			
12	Jianli	12	Hankou			
13	Chenglingji	13	Tianxing			
14	Luoshan	14	Dongcao			
15	Xiantao	15	Dajia	Period number	Impounded water level	Included years
16	Hankou	16	Zhangjia	1	—	—2002
17	Jiujiang			2	135.0–139.0 m	2003–2005
					144.0–156.0 m	2006–2007
					145.0–172.8 m	2008
18	Hukou			3	145.0–171.4 m	2009
					145.0–175.0 m	2010–present

3.3. Channel and Floodplain Resistance Calculation

Manning's roughness coefficient (n) is usually used as a measure of the frictional resistance imposed by natural channels. The total resistance in the MYR was computed using HEC-RAS (Wang & Zhang, 2019), with the observed cross-sectional profiles, average daily discharge, and average daily water level used as river boundary conditions. However, the total resistance (n) alone cannot adequately explain the different contributions of channel and floodplain resistance to low-flow and high-flow water levels. Thus, in low-flow inundation extents, a semi-empirical channel resistance equation has been proposed for large alluvial rivers that considers actual physical conditions based on topography and flow (Nikuradse, 1933; Van Rijn, 1984). Channel resistance (n_c) can be characterized as follows:

Table 2
Sources of Measurements

Data type	Number (station/floodplain/channel)	Period of record	Sources
Daily discharge	Station 1–18	1991–2015	CWRC
Daily water level	Station 1–8	1991–2015	CWRC
Daily sediment concentration	Station 1–18	1991–2015	CWRC
Surveyed profiles	Sub-reach 1–9 (450 cross-section profiles per year)	2004, 2006, 2009, 2012, 2015	CWRC
Surveyed terrains	Sub-reach 1–9 (two-dimensional terrain)	2015	CWRC
Medium diameters of bed load	Station 1, 3, 8, 12, 14, 16	2003–2019	CWRC
Landsat images	Floodplain 1–16	2003, 2004, 2005, 2014, 2015	USGS

$$n_c = \frac{h^{1/6}}{\gamma \lg \left(\frac{12h}{k_s} \right)} \quad (2)$$

where γ denotes the empirical parameter used to consider the bed geometry, which can be calibrated using Equation 3; h is the water depth; and k_s is the equivalent roughness height. However, the form of Equation 2 is similar to the combination of the log law and Manning equation, resulting in a well-known functional relation between the roughness parameters n_c and k_s :

$$\gamma = \frac{h^{1/6}}{n_c \lg \left(\frac{12h}{k_s} \right)} \quad (3)$$

where the parameters on the right side of the equation can be obtained through field data (to obtain h and k_s) and numerical models (to obtain n_c); and k_s is the total roughness height of the dunes (k_{sd}) and riverbed grains (k_{sg}). Dune roughness height (k_{sd}) was calculated from the topographical data using the spent zero-crossing method (IAHR, 1989), which reflects the contribution of riverbed fluctuations to channel resistance. We specified the grain roughness height (k_{sg}) as three times the grain median diameter (D_{50}) (Van Rijn, 1984).

For high-flow inundation extents, we calculated floodplain resistance (n_b) using the Einstein hydraulic radius segmentation method (Einstein & Barbarossa, 1952), which is widely used in resistance segmentation, as follows:

$$n_b = \left(\frac{n_c^{\frac{3}{2}} w - n_c^{\frac{3}{2}} w_c}{w_b} \right)^{\frac{2}{3}} \quad (4)$$

where w , w_b , and w_c are the wet perimeters of the entire cross-section, floodplains, and channel, respectively.

3.4. Determination of Specific Discharges

The trends in water-level variations in the low- and high-flow inundation extents (stages at a given small or large discharge) vary spatially in the MYR. As specific-gauge analysis is often utilized to quantify changes in the stage-discharge relationship over time, the specific discharges of low-flow and high-flow were selected at each hydrometric station (Bormann et al., 2011; Pinter & Heine, 2005) based on the following criteria: (a) discharges must cover both dry and flood events and reflect the morphological changes in the river channel and variations of vegetations in floodplains; and (b) discharge data exist for most years to obtain sufficiently long-term time series of water-levels (Chai et al., 2020). Following these criteria, the specific low- (6,200–12,000 m³/s) and high-flow (31,000–50,000 m³/s) inundation extent discharge threshold values at stations 1, 3, 8, 12, 14, 16, and 17 were determined, respectively (Table 3). Meanwhile, the exceedance probabilities of low- and high-flow inundation extent at each station from 1991 to 2015 were stated in Table 3. The mean exceedance probabilities of low- and high-flow inundation extents in the MYR were 68%–78% and 2%–4%, respectively. Thus, we define the water level of the low- and high-flow inundation extent at each hydrometric station (stations 1, 3, 8, 12, 14, 16, and 17) as the corresponding water level in a given threshold discharge. Additionally, discharges of 30,000 and 35,000 m³/s were selected at stations 1 and 14, respectively, as the bank-full discharges based on the standards specified in CWRC (2021) and Han et al. (2017).

4. Results

4.1. Variations in Water Levels

Figure 2 shows the stage-discharge relationships and variations in water levels in the low- and high-flow inundation extents (stages at a given small or large discharge) from period 1 to period 3 at hydrometric stations 1, 3, 8, 12, 14, 16, and 17. These results indicate that the water levels in the low-flow inundation extents decreased (trend line slope ranges between −0.10 and −0.04 and R^2 ranges between 0.40 and 0.89), whereas those in the high-flow inundation extents showed no decline (trend line slope ranges between −0.01 and 0.03 and $R^2 \leq 0.10$) between

Table 3

Discharges of Low- and High-Flow Inundation Extents and Their Corresponding Exceedance Probabilities at Different Hydrometric Stations From 1991 to 2015

	Station number	1	3	8	12	14	16	17
Low-flow inundation extent	Discharge (m ³ /s)	6,200	6,500	6,500	6,500	10,000	12,000	12,000
	Exceedance probability in period 1	67%	64%	67%	67%	76%	75%	79%
	Exceedance probability in period 2	65%	65%	67%	66%	74%	73%	76%
	Exceedance probability in period 3	76%	78%	74%	77%	76%	76%	78%
	Mean exceedance probability	69%	68%	69%	69%	76%	75%	78%
High-flow inundation extent	Discharge (m ³ /s)	40,000	40,000	33,000	31,000	45,000	50,000	50,000
	Exceedance probability in period 1	3%	4%	4%	4%	7%	6%	6%
	Exceedance probability in period 2	2%	2%	3%	2%	1%	2%	3%
	Exceedance probability in period 3	1%	1%	1%	1%	1%	1%	2%
	Mean exceedance probability	2%	3%	3%	3%	4%	4%	4%

Note. Periods 1–3 indicate periods from 1991 to 2002, 2003 to 2008, and 2009 to 2015, respectively.

periods 1 and 3 at all stations. Such trends are more notable in the reaches nearer the TGD, and the low-flow stages continue to decrease while the high-flow stages slightly increase following adjustment to the operation of the TGD.

To refine the water-level changes (stages at a given small or large discharge) in time and space, the annual water levels in the low- and high-flow inundation extents of each station were analyzed. The low-flow stages decreased between periods 1 and 3 along the MYR, although they slightly rose between 1998 and 1999 due to channel depositions during flood years. Although the decreasing trends were significant at most stations, stations 12 and 17 showed relatively high volatility. Such fluctuations mainly stemmed from the jacking force of Dongting Lake (located near Station 12) and Poyang Lake (located near Station 17). Overall, the low-flow water levels have shown reductions of 0.67, 0.52, 1.27, 0.67, 0.63, 0.75, and 0.84 m at stations 1, 3, 8, 12, 14, 16, and 17, respectively, from the pre-TGD period to the post-TGD period (Figure 2).

However, in comparison to low-flow inundation extents, the water-level variations in high-flow inundation extents are more complicated. Specifically, high-flow water levels (stages at a given large discharge; Figure 1c) slightly increased at stations 1, 8, and 12, stabilized at stations 14, 16, and 17, and slightly decreased at station 3 between periods 1 and 3. At the same time, the observed water-level variations at these stations were minor, generally <0.1 m except for a 0.14-m increase at station 1 (Figures 2 and 6).

Considering the different water-level variations and their underlying mechanism in the low- and high-flow inundation extents after the TGD operation, it is important to distinguish between the influences of the channel and floodplains, respectively. Thus, the impacts of adjustments in channel geomorphology, channel resistance, and floodplain resistance, were examined further.

4.2. Impact of Adjustments in Channel Geomorphology

Figure 3a shows the variations in the cumulative erosion volume of the low- and high-flow inundation extents (erosions at a given small or large discharge) in the MYR between 2003 and 2020 at 2.55 and 0.21 billion m³ for channels and floodplains, respectively. Notably, the low-flow inundation extents accounted for 92% of the total volume, indicating that scouring was mainly concentrated in these channels. Figure 3b shows the adjustment process of the unit accumulated volume of channel sediment degradation in the nine sub-reaches. Except for slight aggradation in sub-reaches 8 and 9 during 2003–2004, the dynamic adjustment of the nine sub-reaches shows a clear erosion status. Moreover, the source intensity of sub-reaches 8 and 9 located far from the dam (Figure 1) was slightly higher than that of sub-reach 7 located near the dam owing to its soft and sandy riverbed that can be easily scoured. This reveals that while the riverbed composition plays an important role in controlling erosion intensity (Figure 3b), the distance downstream of the dam is the dominant factor controlling erosion intensity. This is illustrated by high-intensity erosion in those reaches closest to the dam (e.g., sub-reaches 1–6, extending 408 km).

(A) Stage-Discharge (B) Low-flow stage (C) High-flow stage

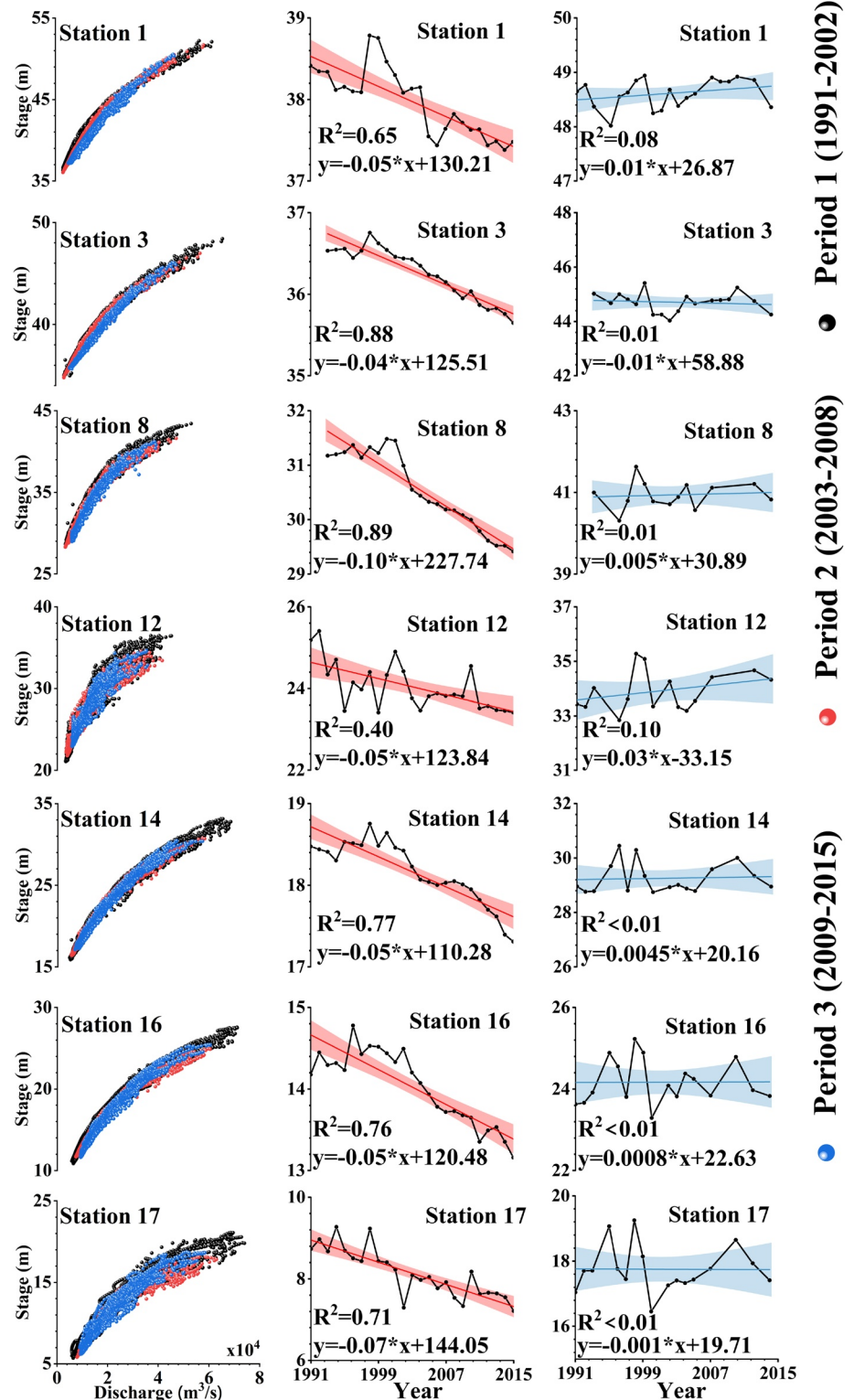


Figure 2. Variations in water-levels at hydrometric stations 1, 3, 8, 12, 14, 16, and 17: (a) Stage-Discharge relationship in period 1 to period 3, (b) trends in low-flow stage over the period of 1991–2015, and (c) trends in high-flow stage over the period of 1991–2015.

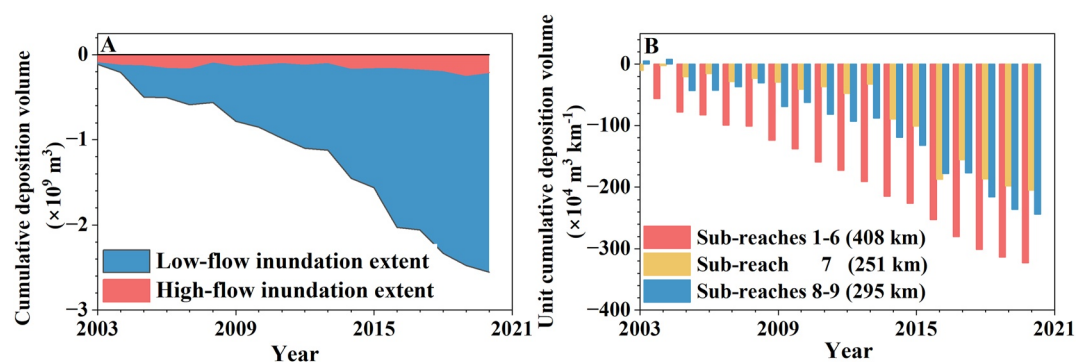


Figure 3. Channel depositions in the Middle Yangtze River: (a) cumulative deposition volume in low-flow (discharge less than $10,000 \text{ m}^3/\text{s}$ at Yichang station) and high-flow inundation extents (discharge over $30,000 \text{ m}^3/\text{s}$ at Yichang station), and (b) cumulative deposition volume per kilometer in each sub-reach. Positive values indicate channel deposition and negative values indicate channel erosion.

Changes in longitudinal profiles of the thalwegs in sub-reaches 1, 2, 3, 7, and 8 from 2004 to 2015 are shown in Figure 4. Since the operation of the TGD, fluctuations of the thalweg profiles have increased, indicating a probably enhanced dune resistance. Except for the sand-gravel bed reach (sub-reach 1), the thalweg adjustments in the near-dam reaches (sub-reaches 2–3) are more dramatic than the far-dam reaches (sub-reaches 7–8).

The nine representative section profiles containing channels and floodplains showed that the riverbeds of the low-flow channels experienced an overall trend of incision, whereas those above the bank-full water level (e.g., stages when discharge = $30,000 \text{ m}^3/\text{s}$ at Station 1) experienced almost no deformation (Figure 5). These morphological changes indicate that the effect of channel erosion on reducing water-level during the low-flow stage was greater than that in the high-flow stage.

The contribution of channel erosion to high-flow water level (stages at a given large discharge) reduction was calculated for the period 2004–2012 under the assumption that resistance was constant. As shown in Figure 6, the topographical changes reduced the flood water level by 0.3–1.5 m, and the corresponding impact of riverbed erosion on the flood water level was weakened due to the reduced erosion downstream.

4.3. Impact of Adjustments in Channel Resistance and Floodplain Resistance

Figure 7 shows that channel and floodplain resistances vary with discharge, time, and space along the MYR. The total resistance displays a decline from upstream to downstream, decreasing from 0.032 at sub-reach 1 to 0.024 (–23%) at sub-reach 9 (Figure 7b). Since the operation of the TGD, the total resistance in the entire MYR has increased from 0.025 in period 2 to 0.029 (+19%) in period 3, and the average increase in total resistance was 59% during this time (period 3 vs. period 2).

Channel resistance increased from 0.022 in period 2 to 0.025 (+12%) in period 3, with the greatest increases occurring in sub-reaches 2–6 due to their fluctuating longitudinal profiles and significant channel geometry adjustments. Floodplain resistance accounted for approximately 65% of the total resistance in the high-flow inundation extents, and the ratios of floodplain resistance to channel resistance in each sub-reach are shown in Figure 7. Floodplain resistance correspondingly increased by 21% (period 3 vs. period 2) as vegetated areas became denser during the post-TGD period.

Unlike floodplain resistance, which only contributed to the water levels during the flood season, channel resistance acts on flows at all times. As severe scouring of the channel results in the arming of bed materials and aggravates channel longitudinal profile fluctuations, grain and dune resistance (components of channel resistance) consequently increase. Figure 8 shows the changes in the equivalent roughness heights and riverbed median diameters in each sub-reach after the operation of the TGD. The overall increase in the equivalent roughness heights was +36%, whereas the growth rate decreased in sub-reaches 1 to 8. Meanwhile, the riverbed median diameters increased by +21%, except for an exceptional increase (+6,545%) in sub-reach 1. Therefore, channel evolution in these reaches is conducive to an increase in channel resistance.

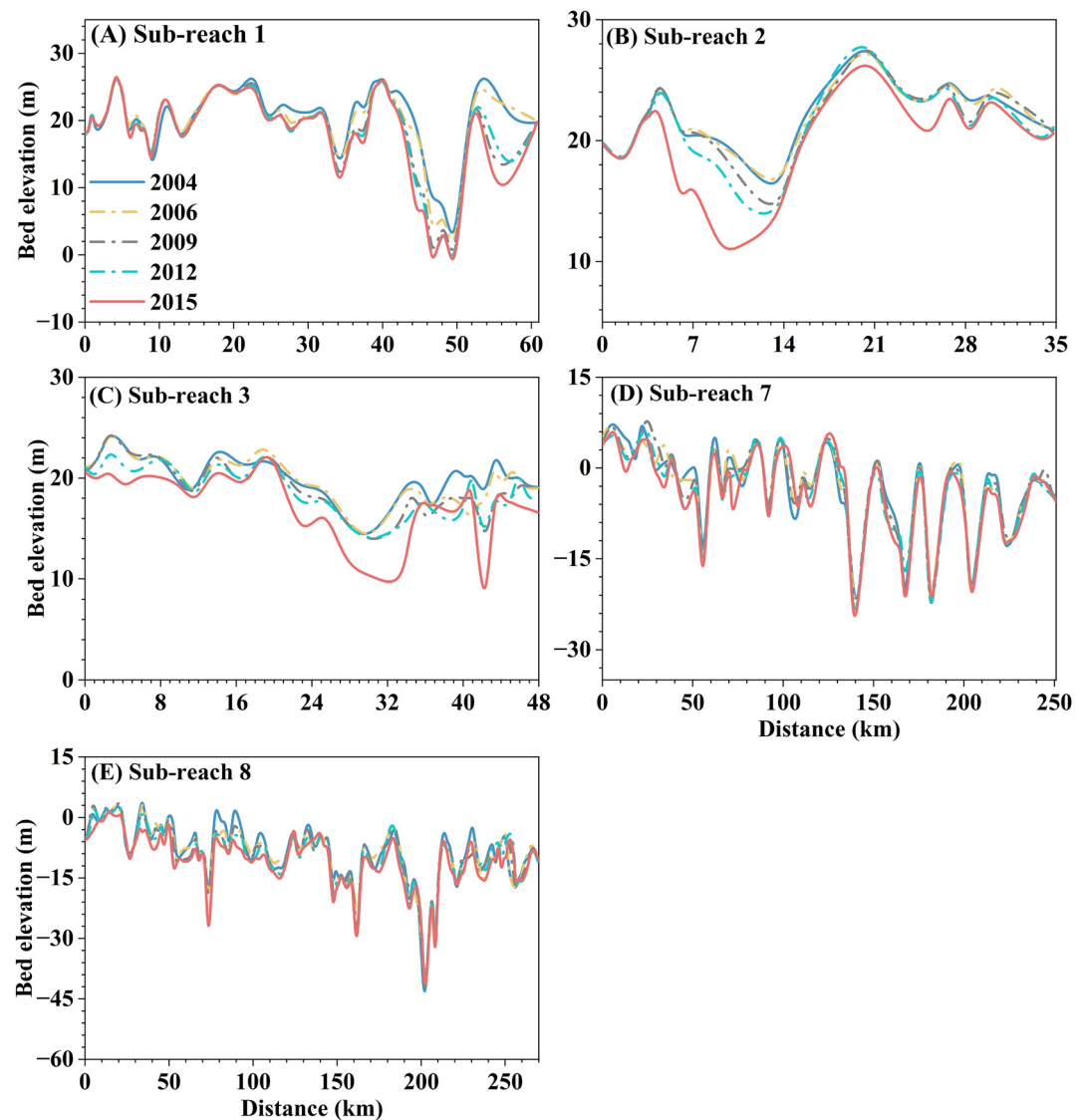


Figure 4. Changes of longitudinal profiles of the thalwegs in sub-reaches 1 (a), 2 (b), 3 (c), 7 (d), and 8 (e), showing notable channel incisions especially in sub-reaches 1–3.

We also calculated the contribution of flow resistance to the increases in high-flow water levels (stages at a given large discharge) between 2004 and 2012 under the assumption of constant terrain. As shown in Figure 9, the total resistance change increased the high-flow water levels by 0.5–1.7 m, and the impact of total resistance on high-flow water levels peaked between hydrometric stations 8 and 13 owing to the concentration of floodplains and developed dunes.

Overall, cumulative erosion in the main channel explains the decreases in water levels in the low-flow inundation extents after the operation of the TGD. Furthermore, increased floodplain resistance largely explains why high-flow water levels were sustained, offsetting the reverse impact of continuous riverbed erosion. Comparatively, channel resistance, which has increased owing to adjustments in channel geomorphology, serves to increase the limited water levels.

5. Discussion

Floodplain resistance is thought to be the main factor driving the observed increase in water levels in the high-flow inundation extents (stages at a given large discharge) of the MYR; however, why and how floodplain resistance has increased following the operation of the TGD remains to be clarified. In addition to the reasons outlined in

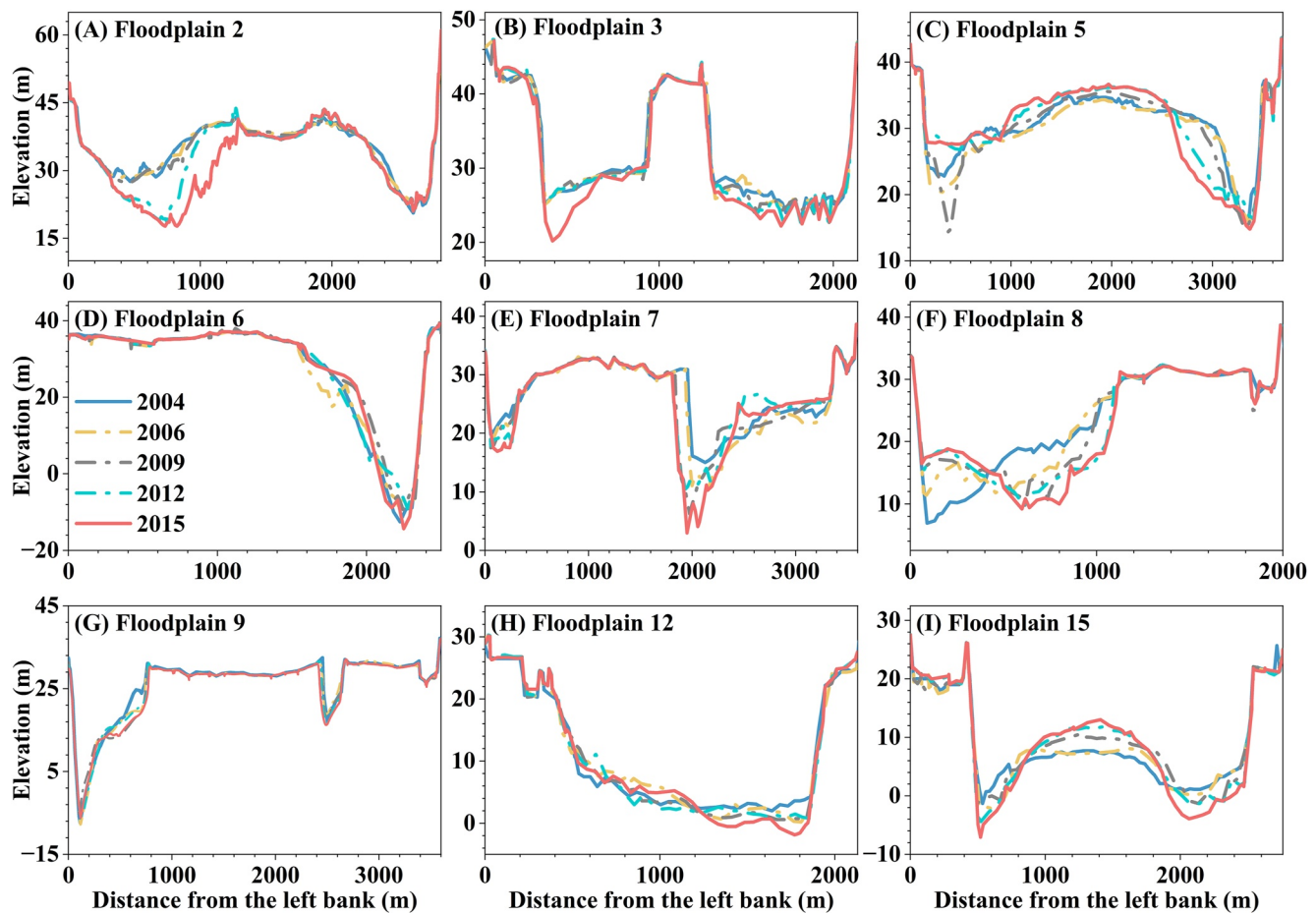


Figure 5. Changes of cross-sectional profiles in the reaches with floodplains (a) 2, (b) 3, (c) 5, (d) 6, (e) 7, (f) 8, (g) 9, (h) 12, and (i) 15.

Sections 4.2 and 4.3, jacking force is also believed to be an important factor increasing the water levels due to the complex river-lake interactions in this region. Previous studies have investigated the range which jacking force can affect and found that the maximum distances of the backwater effects of the Dongting Lake (Sun et al., 2021) and Poyang Lake (Zhang et al., 2022) on the Yangtze River are 264.5 km (sub-reaches 4–6) and 295.4 km (sub-reaches 8–9), respectively. The difference in the jacking forces from Dongting Lake and Poyang Lake after the operation of the TGD may, therefore, help determine whether the higher high-flow water levels were associated with backwater effect.

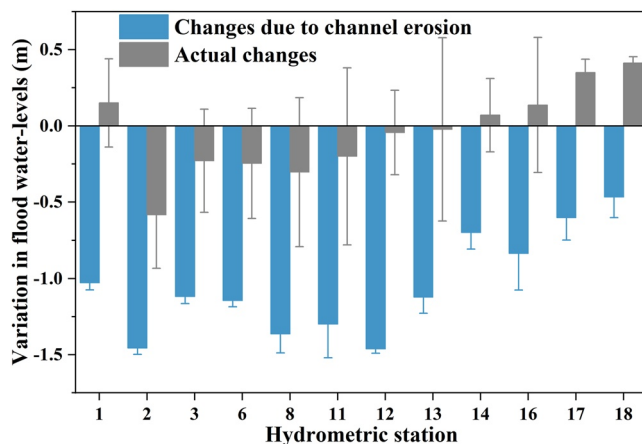


Figure 6. Contributions of topography changes to variations in high-flow water levels (e.g., discharge = 40,000 m³/s at Yichang station) at different hydrometric stations along the Middle Yangtze River from 2004 to 2012.

5.1. Effects of Vegetation

Floodplain resistance is directly related to vegetated areas and is a consequence of the overall effects of floodplain erosion and floodplain submerged frequency (Marjoribanks et al., 2014; Park et al., 2020; Yang et al., 2017). Plant roots are vital for their survival and, therefore, the scouring effect of high flows can result in significant reductions in vegetation cover (Huai et al., 2021). Even when a plant is not uprooted completely by a flood, germination and seedling survival generally depend on a species' flood tolerance (Folkard, 2011). According to our calculations, cumulative floodplain erosion in the MYR was only 0.21 billion m³ between 2003 and 2020, which indicates that floodplain areas—the primary areas of vegetation growth—have eroded very little. Meanwhile, the stage-discharge relationship in a

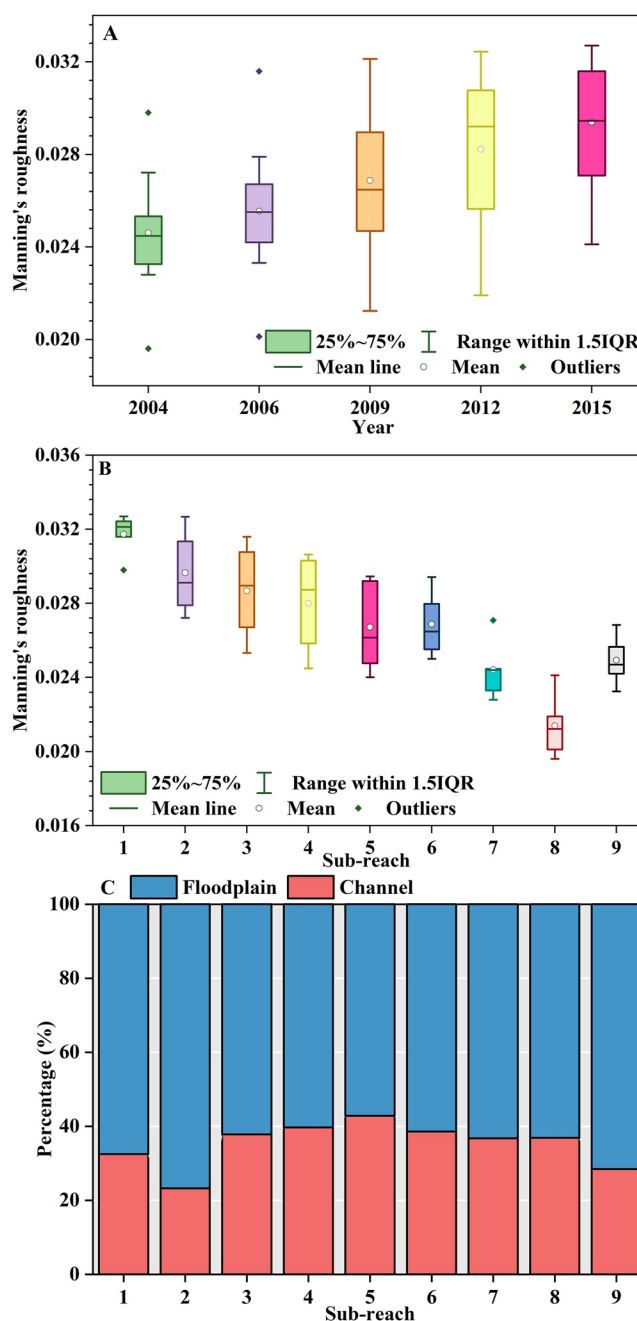


Figure 7. (a) Adjustments of total resistance from 2004 to 2015 in the entire Middle Yangtze River, (b) sub-reaches, and (c) proportions of floodplain resistance and channel resistance.

discharge larger than bank-full discharge remained overall stable (Figure 2, Figures S1 and S2 in Supporting Information S1). Hence, the vegetation-scouring discharges might not change significantly and it will promote vegetation expansion if the exceedance probabilities of vegetation-scouring discharges drop.

A key factor for the elevated floodplain resistance is vegetation expansion, which is thought to have been the primary factor affecting the 2011 Mississippi River (Carle et al., 2015) and likely the dominant role in increasing flood levels in the MYR. The increased resistance was observed with the increased vegetation densities (Figure 11), which can also be reflected through the changes in leaf area index (Box et al., 2021). As vegetated areas increase high-flow water levels (stages at a given large discharge), the characterization of resistance differences between channels and floodplains, and the resulting impact on water levels, is crucial for flood control.

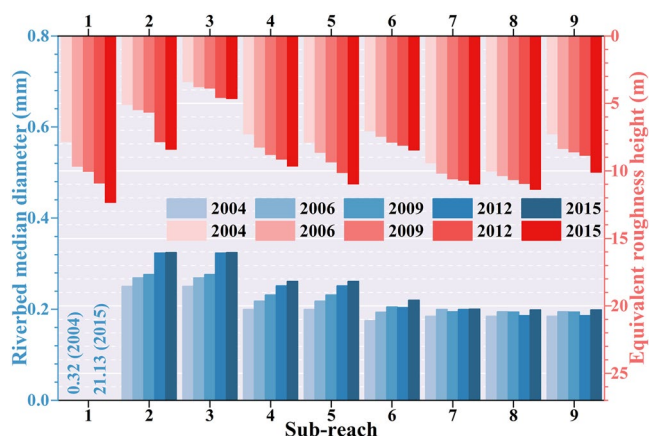


Figure 8. Variation of riverbed sediment median diameters (D_{50}) and equivalent roughness heights (see Equation 2) in different sub-reaches after the operation of the Three Gorges Dam.

Previous studies have also suggested that vegetation growth on floodplains is a function of flood magnitude, frequency, and duration (Carling et al., 2020; Chai et al., 2020; Turner, 1974). Williams and Wolman (1984) regarded the regulation of high flows as the only dam-related factor that was almost certain to encourage vegetation growth. Hence, the floodplain submerged frequencies of all 16 floodplains were investigated between periods 1 to 3, and the corresponding growth of vegetated areas.

We found a significant decrease in the floodplain submerged frequencies of the selected 16 floodplains in the MYR (Figure 10). The operation adjustments of the TGD reduced the floodplain submerged frequency by 34% over 2003–2008 and 19% over 2009–2015, respectively, largely due to a gradual increase in flood inundation. Meanwhile, floodplains in the MYR varied in size (from 2 to 82 km²) and their morphological adjustment during the different periods was relatively minor. There were nevertheless dramatic changes in floodplain extents given that the vast majority of vegetated areas have increased in size (Table 4); this is in response to the increased growth period caused by lower floodplain submerged frequencies.

To further understand the variation of vegetation on the 16 floodplains, we selected two image scenes of Landsat 5 and 8 (near 2003 and 2015) and calculated floodplain areas, vegetated areas, and NDVI values (Figure 11 and Table 4). Vegetation growths were observed in 15 of the 16 selected floodplains. Owing to the expansion of vegetated areas, floodplain resistance has increased. Figure 12 shows the variation in floodplain resistance in each sub-reach along the MYR in two typical flooding years (2004 and 2012) after the operation of the TGD, which shows that in all cases, floodplain resistance increased (average increase = 24%). Sub-reaches 1 and 2 show the most notable increase in floodplain resistance because they are located close to the TGD and were most heavily regulated by the dam; these sub-reaches also have the lowest floodplain submerged frequencies among the MYR. In these areas, the average floodplain resistance was 0.041 during the initial period of the TGD operation, increasing to 0.051 8 years later.

Despite these relationships, a downstream increase in vegetation following the construction of the TGD does not necessarily mean that the dam operation caused this change. As noted by Turner (1974), a number of dam-related factors can affect vegetation. For example, climatic variability complicates any attempt to determine the extent of channel changes and increases in vegetation growth that may be attributable to dams. To clarify whether the floodplain submerged frequency changes were mainly influenced by the TGD regulation, we restored different hydrological processes (i.e., three different TGD regulation methods between period 1 and period 3) at hydro-metric station 1 (the closest station to the TGD, and the most affected by dam regulation) during the period

2010–2015. Our results show that the floodplain submerged frequency was 5.75%, 4.75%, and 3.65% during period 1 (no dam regulation), period 2, and period 3, respectively (Figure 10). In other words, excluding other factors, floodplain submerged frequency decreased immediately following the operation of the TGD. Thus, our data show that reductions in high flows caused by dams contribute significantly to the downstream growth of floodplain vegetation.

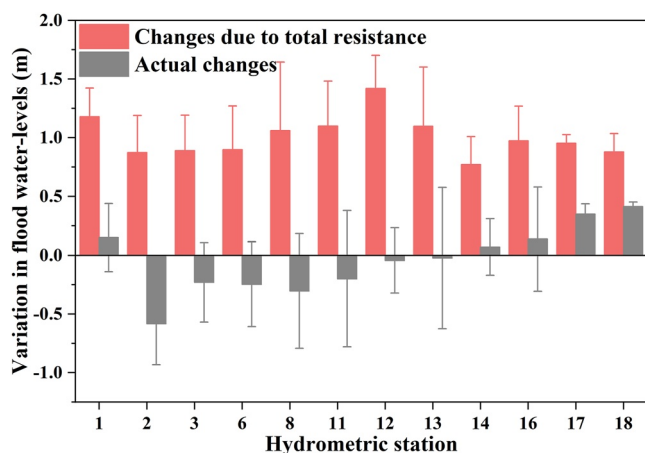


Figure 9. Contributions of total resistance changes to variations in high-flow water levels (e.g., discharge = 40,000 m³/s at Yichang station) at different hydrometric stations along the Middle Yangtze River from 2004 to 2012.

5.2. Effect of Backwater

There are many tributaries in the MYR, with frequent divergence, forming a complicated relationship between rivers, lakes, trunks, and branches. After the impoundment of the TGD and the effects of the incoming flows, adjustment of the reservoir during the year, storage in lakes, and erosion and deposition of the main and branch rivers resulted in the adjustment of the jacking forces between the main and branch streams. Recent research (Chen et al., 2020; Duan et al., 2019; Sun et al., 2021; Zhang et al., 2017) suggests that jacking forces affect the water levels in the mainstream;

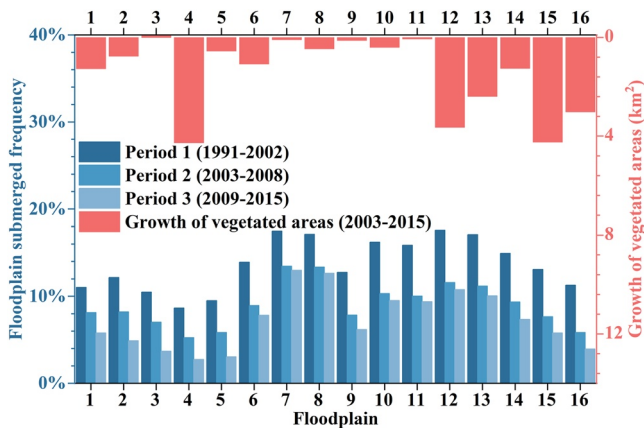


Figure 10. Variation of floodplain submerged frequency and growth of vegetated areas on different floodplains from period 1 to period 3.

however, whether jacking forces increased or decreased after the operation of the TGD requires further discussion. The outflows of Dongting and Poyang Lakes were the main sources of the inflow waters affecting the mainstream of the MYR. The discharge ratio (equal to the discharge in the branch/mainstream) is often used to evaluate the strength of the jacking force (Chen et al., 2020; Sun et al., 2017). Thus, we used the discharge ratio to analyze the inter- and intra-annual variations in the jacking force at the outflow of these two lakes based on daily averaged discharge data from 1991 to 2020. Note that the larger the discharge ratio, the stronger the jacking force.

Figure 13 shows the jacking force associated with Dongting Lake. The main stream of the Yangtze River has a higher discharge rate than the outflow from Dongting Lake as the discharge ratio was <1 on 80% of the studied days, and the annual discharge ratio was ~ 0.65 . Moreover, the jacking force from Dongting Lake continued to decrease between periods 1 and 3 because the discharge ratio frequency increased during the low range $[0, 1]$. Inter-annually, the discharge ratio shows a skewed distribution, being highest from March to June and relatively low from September to December. The

monthly discharge ratio decreased significantly between periods 1 and 3. All monthly discharge ratios in the post-dam periods were <1 , whereas the monthly discharge ratios were >1 from March to May during the pre-dam period. However, the jacking force during flood periods continued to decrease as the discharge ratio frequency gradually decreased in the low range of the discharge ratio (Figure 13c). Thus, the contribution of the jacking

Table 4

Variations of Floodplain Areas, Vegetated Areas, and Average Normalized Difference Vegetation Index Values (NDVI) of the Vegetated Areas of the Floodplains in the Middle Yangtze River Between 2003 and 2015

Floodplain number	Near 2003				Near 2015			
	Time/yy.mm.dd	Floodplain areas/km ²	Vegetated areas/km ²	Mean NDVI	Time/yy.mm.dd	Floodplain areas/km ²	Vegetated areas/km ²	Mean NDVI
1	2003.11.23	2.36	0.28	0.30	2015.12.26	2.47	1.55	0.40
2	2003.11.23	4.15	0.41	0.27	2015.11.01	1.82	1.17	0.49
3	2004.11.02	1.26	0.99	0.52	2015.10.16	1.16	0.91	0.38
4	2004.01.19	5.73	0.11	0.26	2015.01.17	6.01	4.38	0.52
5	2004.11.18	6.44	2.90	0.49	2015.10.16	7.02	3.45	0.48
6	2004.11.02	6.37	5.30	0.41	2015.11.01	7.10	6.38	0.51
7	2004.11.02	7.88	7.27	0.52	2015.11.01	7.89	7.36	0.59
8	2004.11.02	7.27	6.05	0.48	2015.11.01	8.19	6.51	0.58
9	2004.11.02	8.02	7.56	0.44	2015.10.25	8.81	7.68	0.60
10	2003.04.15	10.38	9.86	0.65	2015.04.16	10.98	10.26	0.66
11	2003.04.15	10.31	9.64	0.64	2015.04.16	10.15	9.70	0.63
12	2003.09.22	1.78	1.34	0.46	2015.10.25	6.68	4.98	0.37
13	2003.09.22	15.09	14.00	0.51	2015.10.25	19.82	16.39	0.41
14	2004.04.01	27.51	22.49	0.55	2014.03.05	29.11	23.75	0.52
15	2005.11.07	16.86	12.29	0.27	2015.10.02	18.01	16.53	0.50
16	2002.10.07	82.29	77.10	0.54	2015.10.11	81.68	80.12	0.49

Note. The vegetation is defined by NDVI values and the threshold for vegetation and non-vegetation is 0.2, which means when the NDVI value of a specific pixel is greater than 0.2, this pixel is classified as vegetation in our definition, vice versa. The threshold for floodplain and water is 0, which means when the NDVI value of a specific pixel is greater than 0, this pixel is classified as floodplain. Areas are determined by the products of the pixel counts (i.e., the number of pixels) and the area of one pixel (i.e., 900 m²).

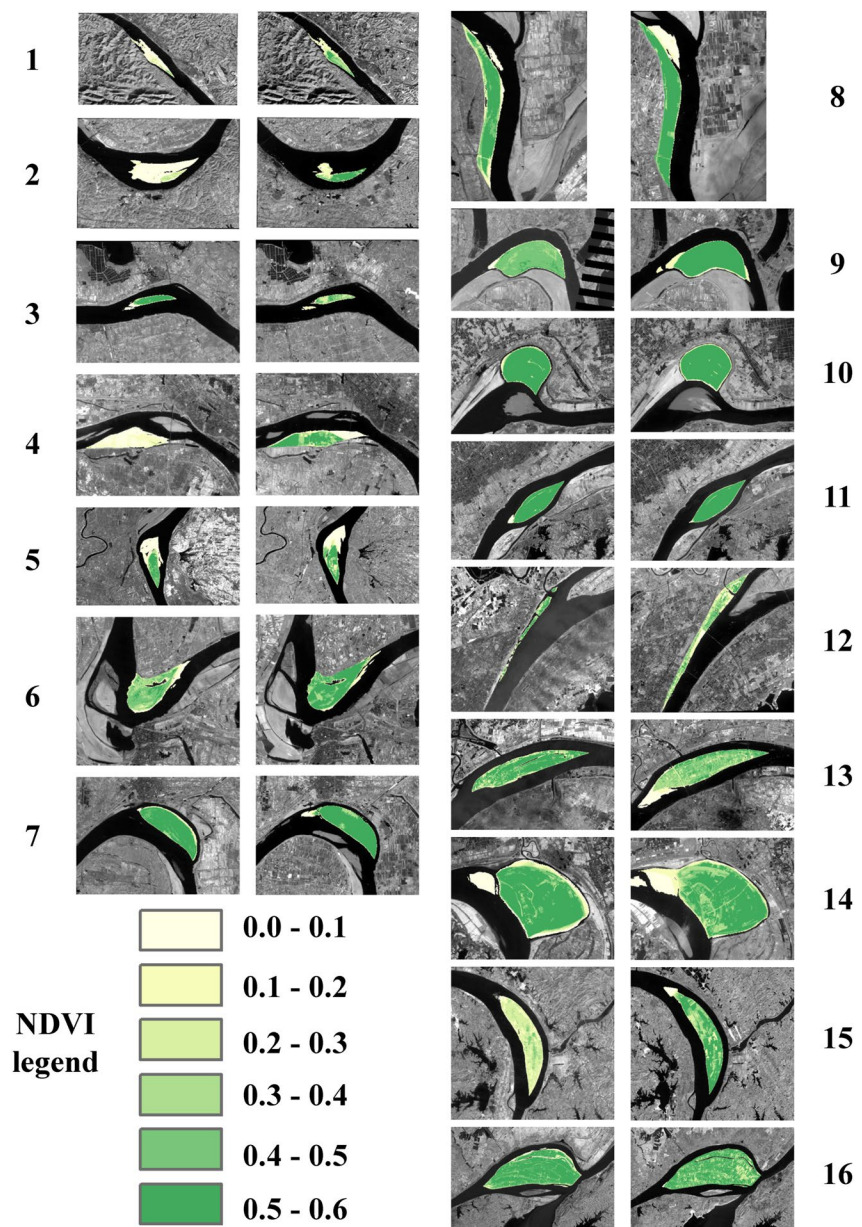


Figure 11. Variations of floodplain vegetation distributions in the Middle Yangtze River in 2003 (left in each panel) and 2015 (right in each panel), respectively. Only the normalized difference vegetation index (NDVI) of floodplains (more green means larger NDVI values) are shown and the backgrounds are shown by the near-infrared band. Black lines in the figure for Floodplain 9 due to missing data in the edge of the image scene of Landsat 5. The numbers on the far left and right are the floodplain numbers.

force from Dongting Lake to the water levels in high-flow inundation extents (stages at a given large discharge) decreased after the operation of the TGD.

Figure 14 shows the jacking force associated with Poyang Lake. The main stream in the Yangtze River also has a higher discharge rate than the outflow from Poyang Lake, with an annual discharge ratio of ~ 0.25 —much smaller than that of Dongting Lake. The jacking force from Poyang Lake continued to decrease between periods 1 and 3 because the discharge ratio frequency decreased in the interval $[0.2, 1]$ but increased in the lower interval $[0, 0.2]$. Similar to Dongting Lake, the inter-annual variation in the discharge ratio of Poyang Lake also shows a skewed distribution, and the monthly discharge ratios notably decreased from periods 1 to 3. All monthly discharge ratios

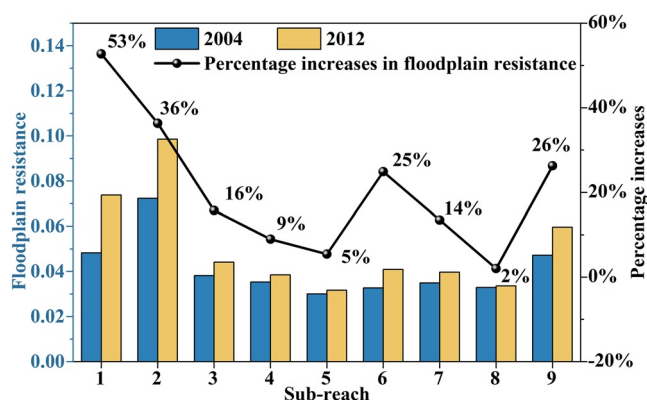


Figure 12. Variations of floodplain resistance and their percentage increases from 2004 to 2012 in each sub-reach.

in the post-dam periods were <0.4 , whereas the monthly discharge ratios were >1 in April during the pre-dam period. However, the jacking forces during flood flows also became lower as the discharge ratio frequency gradually decreased in the low interval of the discharge ratio, especially the frequency of reflowing into the lake (i.e., discharge ratio <0). Thus, the contribution of the jacking force from Poyang Lake to the water levels in high-flow inundation extents (stages at a given large discharge) also decreased after the operation of the TGD. In addition to these two lakes, several small tributaries merge into the Yangtze River, although their associated jacking forces can be disregarded owing to their small discharges.

5.3. Broader Implications

Previous studies have analyzed the water levels in the Yangtze River through the specific-gauge analysis (stages at a given large or small discharge) and investigated possible effects of the TGD operation on low- and high-flow water levels based on hydrological data and numerical modeling (Bormann et al., 2011; Han et al., 2017; Nakayama & Shankman, 2013). Specifically, the decreased low-flow water level is closely associated with channel erosion by the sediment-depleted flow since the TGD operation (Yang et al., 2017). In contrast, there are major controversies in interpreting the insignificant changes in high-flow water levels, though the possible impacts have been pointed out, such as the flow resistance, river-lake relationship, and river regulation works such as dikes and groins (Chai et al., 2020; Han et al., 2017). However, the fact that channel enlargement and vegetation expansion can trigger changes in flow resistance between pre- and post-TGD periods, and between channel and floodplain regions is often not fully considered, despite its potential strong impact on the high-flow water levels. Thus, rather than the intended consequence of reducing high-flow water levels due to bed incision downstream of the TGD, the underlying mechanisms of enhanced channel and floodplain resistance in amplifying flood risks are still uncertain.

The significant test for our quantitative understanding of water-level variations following dam operation lies in our ability to predict regional flood risk and the associated implications of environmental changes (Latrubesse et al., 2017). To address these challenges and to serve as a catalyst to bring about the necessary changes in hydrologic and geomorphologic science, the understanding of the mechanisms controlling these variations must be improved (Best, 2019; Syvitski et al., 2022). In the Yangtze River, water-level variations downstream of the TGD are similar to those observed in other dammed fluvial systems, that is, water levels have decreased in low-flow inundation extents but have not decreased in high-flow inundation extents (stages at a given small or large discharge) (Bormann et al., 2011; Carle et al., 2015; Day et al., 2016; James, 1991; Lai et al., 2014; Li et al., 2018, 2019; Lu, 1994; Pinter & Heine, 2005; Shields et al., 2000; Topping et al., 2003; Yang et al., 2017). While the lower water levels in low-flow inundation extents can be explained by channel erosion, the relatively stable water levels in the high-flow inundation extents require further analysis owing to their associated flood risk. The MYR provides an ideal case study, as it is currently in the process of transitioning in its grain-size, dune, and vegetation response to damming, and its extensive records provide both pre- and post-dam data that are not readily available for most of the world's large rivers. These data enable estimates of changes in channel and floodplain resistance, and their impact on river stage.

As we have previously stressed, increased floodplain resistance is the dominant factor affecting the flood water levels in the MYR owing to the growth of vegetation after the operation of the TGD. This provides support for evaluating many dam-affected rivers, many of which show an expansion in vegetated areas on floodplains (Deng et al., 2014; Zhou et al., 2020) indicating a possible increase in floodplain resistance. For example, in the United States, striking increases in vegetation have occurred in the Arkansas River downstream of John Martin Dam (+90%), the Republican River downstream of Trenton Dam (+55%), the Salt Fork River downstream of Arkansas Dam (+33%), the North Canadian River downstream of Canton Dam (+40%), the Platte River downstream of Kingsley Dam, the Canadian River downstream of Sanford Dam, and the Missouri River downstream of Garrison Dam (Johnson et al., 2012; Williams & Wolman, 1984). Nevertheless, other factors not discussed here but which affect water levels require further investigation, including waterway regulation projects (Yan et al., 2019; Yang et al., 2022).

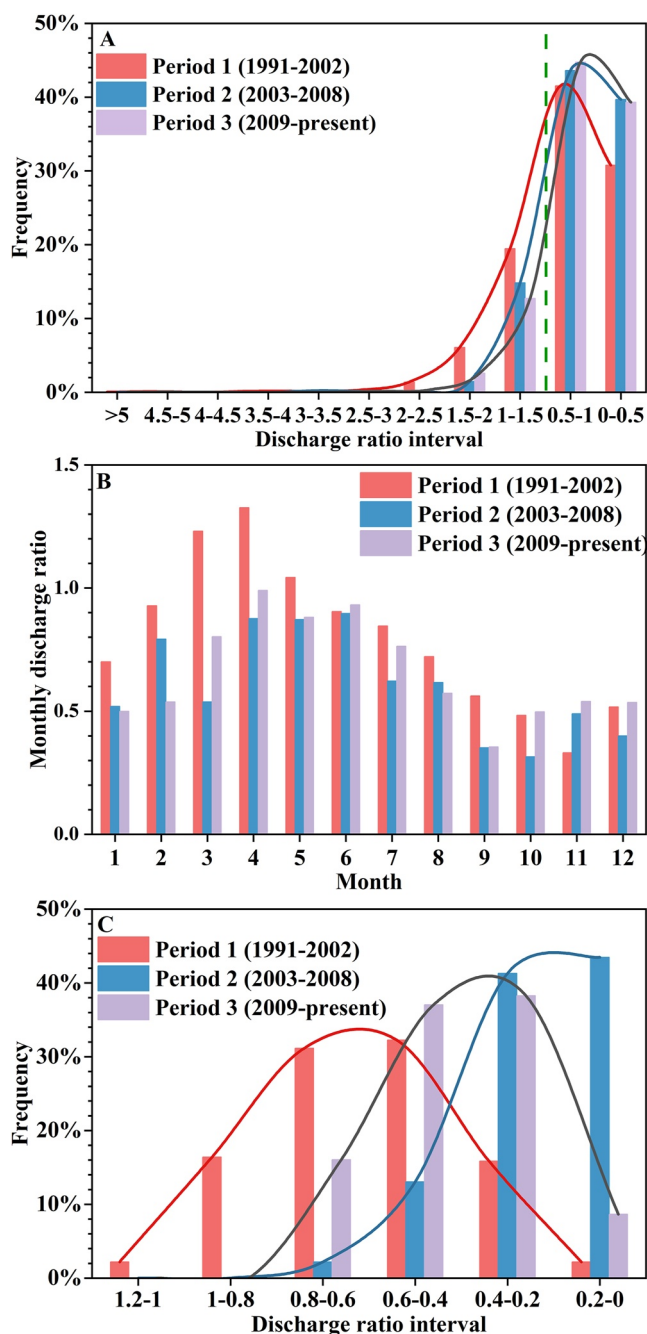


Figure 13. Variations of jacking force from Dongting Lake from period 1 to period 3: (a) the frequency distribution of annual discharge ratio, (b) monthly discharge ratio distribution, and (c) the frequency distribution of discharge ratio when flooding occurs (e.g., discharge = 40,000 m³/s at Yichang station).

6. Conclusions

We have performed a systematic investigation of the mechanisms controlling the water-level variations (stages at a given small or large discharge) in the MYR downstream of the TGD. Our results indicate that the water levels in low-flow inundation extents decreased substantially since the operation of the TGD largely due to intensive channel erosion. By contrast, the water levels in high-flow inundation extents remained stable and even showed slight increases from period 1 (1991–2002) to period 2 (2003–2008) and period 3 (2009–2015) at all hydrometric stations. Such anomalous changes in high-flow water levels are mainly driven by an increase in total resistance. Under flood flows, floodplain resistance contributes ~65% of the total resistance owing to the expansion of

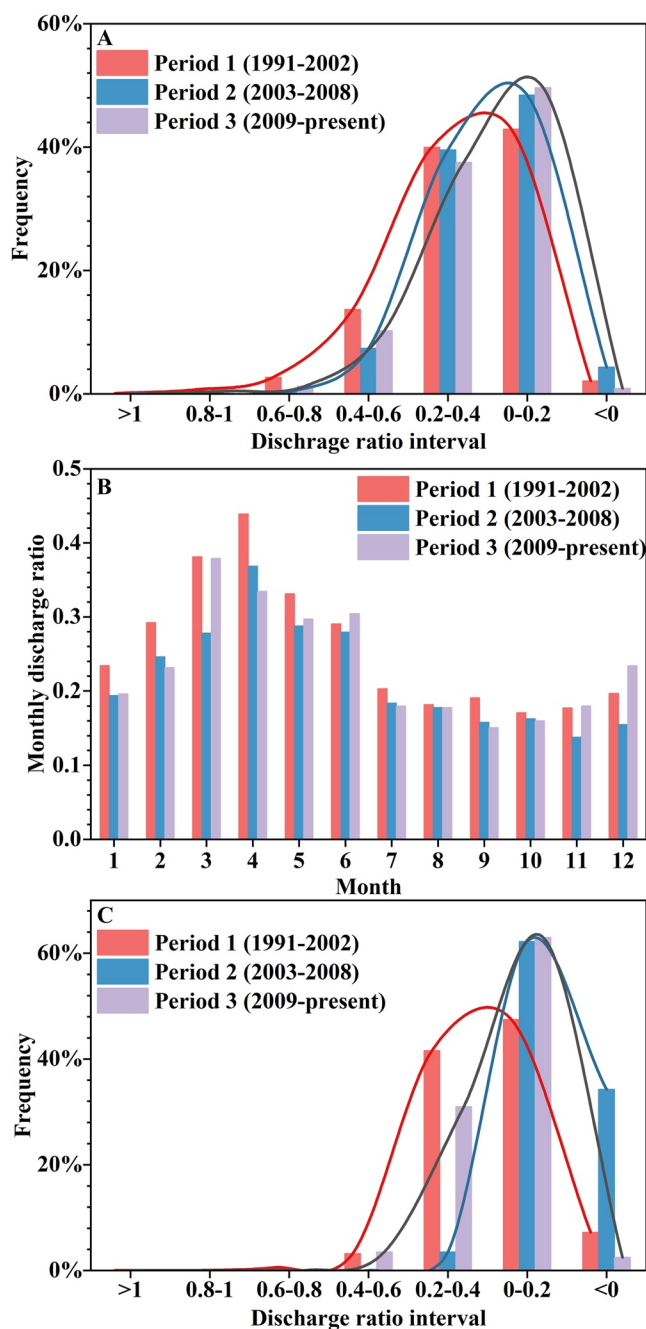


Figure 14. Variations of jacking force from Poyang Lake from period 1 to period 3: (a) annual discharge ratio frequency distribution, (b) monthly discharge ratio distribution, and (c) discharge ratio frequency distribution when flooding occurs (e.g., discharge = 40,000 m³/s at Yichang station).

vegetated areas on floodplains, followed by riverbed coarsening and greater fluctuations in the river longitudinal profile. Therefore, the operation of the TGD have exerted substantial influences on downstream water-level variations. We suggest that the appropriate adjustments of the operation mode of the TGD should be adopted to help mitigate flood risk within the basin that is home to over 400 million people.

Conflict of Interest

The authors declare no conflicts of interest relevant to this study.

Data Availability Statement

The data that support the findings of this study are openly available at the following URL: <https://data.mendeley.com/datasets/zcvtwpfj4z/1>.

Acknowledgments

The authors gratefully thank Editor Ellen Wohl, anonymous Associate Editor, and reviewers for their valuable and constructive comments in improving this study. This work was supported by the National Natural Science Foundation of China (Grant No. 51779185), and the National Key R&D Program of China (Grant No. 2018YFC0407201).

References

- Best, J. (2019). Anthropogenic stresses on the world's big rivers. *Nature Geoscience*, 12(1), 7–21. <https://doi.org/10.1038/s41561-018-0262-x>
- Bormann, H., Pinter, N., & Elfert, S. (2011). Hydrological signatures of flood trends on German rivers: Flood frequencies, flood heights and specific stages. *Journal of Hydrology*, 404(1–2), 50–66. <https://doi.org/10.1016/j.jhydrol.2011.04.019>
- Box, W., Järvelä, J., & Västilä, K. (2021). Flow resistance of floodplain vegetation mixtures for modelling river flows. *Journal of Hydrology*, 601, 126593. <https://doi.org/10.1016/j.jhydrol.2021.126593>
- Cao, G. J., & Wang, J. (2015). *Measurements and studies of hydrological and sediment data in the Three Gorges Project*. Science Press.
- Carle, M. V., Sasser, C. E., & Roberts, H. H. (2015). Accretion and vegetation community change in the Wax Lake Delta following the historic 2011 Mississippi River flood. *Journal of Coastal Research*, 31(3), 569–587. <https://doi.org/10.2112/jcoastres-d-13-00109.1>
- Carling, P. A., Leyland, J., Kleinhans, M. G., Besozzi, L., Duranton, P., Trieu, H., & Teske, R. (2020). Quantifying fluid retention due to natural vegetation in a forest floodplain analogue using the aggregated dead zone (ADZ) dilution approach. *Water Resources Research*, 56(9), e2020WR027070. <https://doi.org/10.1029/2020wr027070>
- Chai, Y., Yang, Y., Deng, J., Sun, Z., Li, Y., & Zhu, L. (2020). Evolution characteristics and drivers of the water level at an identical discharge in the Jingjiang reaches of the Yangtze River. *Journal of Geographical Sciences*, 30(10), 1633–1648. <https://doi.org/10.1007/s11442-020-1804-x>
- Chen, D., Qu, G., Guo, X., & Yu, M. (2020). Study of the supporting and falling impact of Dongting Lake on the lower Jingjiang river before and after construction of three Gorges Dam. *Advanced Engineering Sciences*, 52(2), 86–94.
- CWRC. (2021). *Analysis of channel degradation downstream of the three Gorges dam*. Scientific Report.
- Darby, S. E., Hackney, C. R., Leyland, J., Kumm, M., Lauri, H., Parsons, D. R., et al. (2016). Fluvial sediment supply to a mega-delta reduced by shifting tropical-cyclone activity. *Nature*, 539(7628), 276–279. <https://doi.org/10.1038/nature19809>
- Day, J. W., Cable, J. E., Lane, R. R., & Kemp, G. P. (2016). Sediment deposition at the Caernarvon crevasse during the great Mississippi flood of 1927: Implications for coastal restoration. *Water*, 8(2), 38. <https://doi.org/10.3390/w8020038>
- Deng, F., Wang, X., Cai, X., Li, E., Jiang, L., Li, H., & Yan, R. (2014). Analysis of the relationship between inundation frequency and wetland vegetation in Dongting Lake using remote sensing data. *Ecology*, 95(2), 717–726. <https://doi.org/10.1002/eco.1393>
- Doyle, M. W., & Harbor, J. M. (2003). A scaling approximation of equilibrium timescales for sand-bed and gravel-bed rivers responding to base-level lowering. *Geomorphology*, 54(3–4), 217–223. [https://doi.org/10.1016/S0169-555X\(02\)00357-4](https://doi.org/10.1016/S0169-555X(02)00357-4)
- Duan, Y. X., Li, J. B., Lv, D. Q., Wang, D. Y., Dai, W., & Liu, W. (2019). Hydrological conditions and the mutual supporting effects at the intersection area of Dongting Lake and Yangtze River under the operation of the three Gorges reservoir. *Resources and Environment in the Yangtze Basin*, 28(10), 2471–2483.
- Einstein, H. A., & Barbarossa, N. L. (1952). River channel roughness. *Transactions of the American Society of Civil Engineers*, 117(1), 1121–1132. <https://doi.org/10.1061/taceat.0006666>
- Folkard, A. M. (2011). Vegetated flows in their environmental context: A review. *Proceedings of the Institution of Civil Engineers-Engineering and Computational Mechanics*, 164(1), 3–24. <https://doi.org/10.1680/jecm.8.00006>
- Gierszewski, P. J., Habel, M., Szmańda, J., & Luc, M. (2020). Evaluating effects of dam operation on flow regimes and riverbed adaptation to those changes. *Science of the Total Environment*, 710, 136202. <https://doi.org/10.1016/j.scitotenv.2019.136202>
- Han, J., Sun, Z., Li, Y., & Yang, Y. (2017). Combined effects of multiple large-scale hydraulic engineering on water stages in the Middle Yangtze River. *Geomorphology*, 298, 31–40. <https://doi.org/10.1016/j.geomorph.2017.09.034>
- He, Z., Sun, Z., Li, Y., Zhao, Q., Hu, Y., & Chen, Z. (2021). Response of the gravel–sand transition in the Yangtze River to hydrological and sediment regime changes after upstream damming. *Earth Surface Processes and Landforms*, 47(2), 383–398. <https://doi.org/10.1002/esp.5254>
- Huai, W. X., Li, S., Katul, G. G., Liu, M. Y., & Yang, Z. H. (2021). Flow dynamics and sediment transport in vegetated rivers: A review. *Journal of Hydrodynamics*, 33(3), 400–420. <https://doi.org/10.1007/s42241-021-0043-7>
- IAHR Working Group on Wave Generation and Analysis. (1989). List of sea-state parameters. *Journal of Waterway, Port, Coastal, and Ocean Engineering*, 115(6), 793–808. [https://doi.org/10.1061/\(asce\)0733-950x\(1989\)115:6\(793\)](https://doi.org/10.1061/(asce)0733-950x(1989)115:6(793))
- James, L. A. (1991). Incision and morphologic evolution of an alluvial channel recovering from hydraulic mining sediment. *The Geological Society of America Bulletin*, 103(6), 723–736. [https://doi.org/10.1130/0016-7606\(1991\)103<0723:iameoa>2.3.co;2](https://doi.org/10.1130/0016-7606(1991)103<0723:iameoa>2.3.co;2)
- Jemberie, A. A., Pinter, N., & Remo, J. W. (2008). Hydrologic history of the Mississippi and Lower Missouri Rivers based upon a refined specific-gauge approach. *Hydrological Processes: International Journal*, 22(22), 4436–4447. <https://doi.org/10.1002/hyp.7046>
- Johnson, W. C., Dixon, M. D., Scott, M. L., Rabbe, L., Larson, G., Volke, M., & Werner, B. (2012). Forty years of vegetation change on the Missouri River floodplain. *BioScience*, 62(2), 123–135. <https://doi.org/10.1525/bio.2012.62.2.6>
- Lai, X., Jiang, J., Yang, G., & Lu, X. X. (2014). Should the Three Gorges Dam be blamed for the extremely low water levels in the middle–lower Yangtze River? *Hydrological Processes*, 28(1), 150–160. <https://doi.org/10.1002/hyp.10077>
- Latrubesse, E. M., Arima, E. Y., Dunne, T., Park, E., Baker, V. R., d'Horta, F. M., et al. (2017). Damming the rivers of the Amazon basin. *Nature*, 546(7658), 363–369. <https://doi.org/10.1038/nature22333>
- Leopold, L. B. (1956). Land use and sediment. *Man's Role in Changing the Face of the Earth*, 2, 639–647.
- Li, D., Lu, X., Overeem, I., Walling, D. E., Syvitski, J., Kettner, A. J., et al. (2021). Exceptional increases in fluvial sediment fluxes in a warmer and wetter High Mountain Asia. *Science*, 374(6567), 599–603. <https://doi.org/10.1126/science.abi9649>
- Li, D., Lu, X., Walling, D. E., Zhang, T., Steiner, J. F., Wasson, R. J., et al. (2022). High Mountain Asia hydropower systems threatened by climate-driven landscape instability. *Nature Geoscience*, 15(7), 520–530. <https://doi.org/10.1038/s41561-022-00953-y>
- Li, D., Lu, X. X., Chen, L., & Wasson, R. J. (2019). Downstream geomorphic impact of the three Gorges Dam: With special reference to the channel bars in the Middle Yangtze River. *Earth Surface Processes and Landforms*, 44(13), 2660–2670. <https://doi.org/10.1002/esp.4691>
- Li, D., Lu, X. X., Yang, X., Chen, L., & Lin, L. (2018). Sediment load responses to climate variation and cascade reservoirs in the Yangtze River: A case study of the Jinsha river. *Geomorphology*, 322, 41–52. <https://doi.org/10.1016/j.geomorph.2018.08.038>
- Lu, J. Y. (1994). Variation of stage-discharge relationship of downstream of hydro-junction. *Journal of Nanjiang Hydraulic Research Institute*, 1, 109–117.

- Lyu, Y., Fagherazzi, S., Zheng, S., Tan, G., & Shu, C. (2020). Enhanced hysteresis of suspended sediment transport in response to upstream damming: An example of the Middle Yangtze River downstream of the Three Gorges Dam. *Earth Surface Processes and Landforms*, 45(8), 1846–1859. <https://doi.org/10.1002/esp.4850>
- Ma, H., Nittrouer, J. A., Fu, X., Parker, G., Zhang, Y., Wang, Y., et al. (2022). Amplification of downstream flood stage due to damming of fine-grained rivers. *Nature Communications*, 13(1), 1–11. <https://doi.org/10.1038/s41467-022-30730-9>
- Marjoribanks, T. I., Hardy, R. J., & Lane, S. N. (2014). The hydraulic description of vegetated river channels: The weaknesses of existing formulations and emerging alternatives. *Wiley Interdisciplinary Reviews: Water*, 1(6), 549–560. <https://doi.org/10.1002/wat2.1044>
- Nakayama, T., & Shankman, D. (2013). Impact of the Three-Gorges Dam and water transfer project on Changjiang floods. *Global and Planetary Change*, 100, 38–50. <https://doi.org/10.1016/j.gloplacha.2012.10.004>
- Nikuradse, J. (1933). Stromungsgesetze in rauen Rohren. *vdi-forschungsheft*, 361, 1.
- Park, E. (2020). Characterizing channel-floodplain connectivity using satellite altimetry: Mechanism, hydrogeomorphic control, and sediment budget. *Remote Sensing of Environment*, 243, 111783. <https://doi.org/10.1016/j.rse.2020.111783>
- Park, E., Ho, H. L., Tran, D. D., Yang, X., Alcantara, E., Merino, E., & Son, V. H. (2020). Dramatic decrease of flood frequency in the Mekong Delta due to river-bed mining and dyke construction. *Science of the Total Environment*, 723, 138066. <https://doi.org/10.1016/j.scitotenv.2020.138066>
- Pinter, N., & Heine, R. A. (2005). Hydrodynamic and morphodynamic response to river engineering documented by fixed-discharge analysis, Lower Missouri River, USA. *Journal of Hydrology*, 302(1–4), 70–91. <https://doi.org/10.1016/j.jhydrol.2004.06.039>
- Pinter, N., Jemberie, A. A., Remo, J. W., Heine, R. A., & Ickes, B. S. (2008). Flood trends and river engineering on the Mississippi River system. *Geophysical Research Letters*, 35(23), L23404. <https://doi.org/10.1029/2008gl035987>
- Schmitt, R. J., Bizzi, S., Castelletti, A., & Kondolf, G. M. (2018). Improved trade-offs of hydropower and sand connectivity by strategic dam planning in the Mekong. *Nature Sustainability*, 1(2), 96–104. <https://doi.org/10.1038/s41893-018-0022-3>
- Shields, F. D., Jr., Simon, A., & Steffen, L. J. (2000). Reservoir effects on downstream river channel migration. *Environmental Conservation*, 27(1), 54–66. <https://doi.org/10.1017/s0376892900000072>
- Sun, Z., Li, Q., Yan, X., & Luo, F. (2017). Analysis of the critical relationship between the water levels of Dongting Lake and Chenglingji station. *Advances in Water Science*, 28(4), 496–506.
- Sun, Z., Zhou, X., Fan, J., Xiong, H., & Tan, G. (2021). Stage-discharge rating method considering backwater effect in river channel. *Advances in Water Science*, 32(2), 259–270.
- Syvitski, J., Ángel, J. R., Saito, Y., Overeem, I., Vörösmarty, C. J., Wang, H., & Olago, D. (2022). Earth's sediment cycle during the Anthropocene. *Nature Reviews Earth & Environment*, 3(3), 1–18. <https://doi.org/10.1038/s43017-021-00253-w>
- Topping, D. J., Schmidt, J. C., & Vierra, L. E. (2003). *Computation and analysis of the instantaneous-discharge record for the Colorado river at Lees Ferry, Arizona — May 8, 1921, through September 30, 2000*. U.S. Geological Survey.
- Turner, R. M. (1974). *Quantitative and historical evidence of vegetation changes along the upper Gila River, Arizona*. U.S. Geological Survey Professional Paper.
- Van Rijn, L. C. (1984). Sediment transport, part III: Bed forms and alluvial roughness. *Journal of Hydraulic Engineering*, 110(12), 1733–1754. [https://doi.org/10.1061/\(asce\)0733-9429\(1984\)110:12\(1733\)](https://doi.org/10.1061/(asce)0733-9429(1984)110:12(1733))
- Wang, J., & Zhang, Z. (2019). Evaluating riparian vegetation roughness computation methods integrated within HEC-RAS. *Journal of Hydraulic Engineering*, 145(6), 04019020. [https://doi.org/10.1061/\(asce\)hy.1943-7900.0001597](https://doi.org/10.1061/(asce)hy.1943-7900.0001597)
- Williams, G. P., & Wolman, M. G. (1984). *Downstream effects of dams on alluvial rivers*. US Government Printing Office.
- Xia, J., Deng, S., Lu, J., Xu, Q., Zong, Q., & Tan, G. (2016). Dynamic channel adjustments in the Jingjiang reach of the Middle Yangtze River. *Scientific Reports*, 6(1), 1–10. <https://doi.org/10.1038/srep22802>
- Xia, J., Zhou, M., Lin, F., Deng, S., & Lu, J. (2017). Variation in reach-scale bankfull discharge of the Jingjiang Reach undergoing upstream and downstream boundary controls. *Journal of Hydrology*, 547, 534–543. <https://doi.org/10.1016/j.jhydrol.2017.02.026>
- Yan, T., Yang, Y. P., Li, Y. B., Chai, Y. F., & Cheng, X. B. (2019). Possibilities and challenges of expanding dimensions of waterway downstream of Three Gorges Dam. *Water Science and Engineering*, 12(2), 136–144. <https://doi.org/10.1016/j.wse.2019.05.004>
- Yang, Y., Liu, W., Zhang, J., Yang, L., Jia, M., & Zhu, L. (2022). Changes of divergence and confluence relationship between Dongting Lake and the Yangtze River after the operation of the three Gorges project and its impact on the waterway depth. *Frontiers of Earth Science*, 84. <https://doi.org/10.3389/feart.2022.829669>
- Yang, Y., Zhang, M., Zhu, L., Liu, W., Han, J., & Yang, Y. (2017). Influence of large reservoir operation on water-levels and flows in reaches below dam: Case study of the Three Gorges Reservoir. *Scientific Reports*, 7(1), 1–14. <https://doi.org/10.1038/s41598-017-15677-y>
- Zhang, M., Deng, P., Wang, L., Bing, J., Zhang, D., & Cheng, X. (2022). Quantitative analysis of influence of converge jacking in Lake Poyang on the water level in Hankou of Yangtze River. *Journal of Lake Sciences*, 34(5), 1712–1722.
- Zhang, W., Yang, Y., Zhang, M., Li, Y., Zhu, L., You, X., et al. (2017). Mechanisms of suspended sediment restoration and bed level compensation in downstream reaches of the Three Gorges Projects (TGP). *Journal of Geographical Sciences*, 27(4), 463–480. <https://doi.org/10.1007/s11442-017-1387-3>
- Zheng, S. (2016). Reflections on the three Gorges project since its operation. *Engineering*, 2(4), 389–397. <https://doi.org/10.1016/j.eng.2016.04.002>
- Zhou, Y., Li, D., Lu, J., Yao, S., Yan, X., Jin, Z., et al. (2020). Distinguishing the multiple controls on the decreased sediment flux in the Jialing River basin of the Yangtze River, Southwestern China. *Catena*, 193, 104593. <https://doi.org/10.1016/j.catena.2020.104593>